applied sciences

MDPI

Article

Modeling and Control of a Nonlinear Dual-Pendulum Energy Harvester Using BLDC Motors and MPPT Algorithm

Marcin Fronc [1,*], Marek Borowiec [2,*], Grzegorz Litak [3], Krzysztof Kolano [1] and Mateusz Waśkowicz [3]

[1] Department of Electrical Drives and Machines, Faculty of Electrical Engineering and Computer Science, Lublin University of Technology, 20-618 Lublin, Poland; k.kolano@pollub.pl
[2] Department of Applied Mechanics, Lublin University of Technology, Nadbystrzycka 36, 20-618 Lublin, Poland
[3] Department of Automation, Faculty of Mechanical Engineering and Computer Science, Lublin University of Technology, 20-618 Lublin, Poland
* Correspondence: m.fronc@pollub.pl (M.F.); m.borowiec@pollub.pl (M.B.)

Abstract

Nonlinear energy harvesting systems based on multibody structures constitute a promising solution for autonomous devices powered by ambient vibrations. This paper presents the modeling and control of a nonlinear energy harvester employing a double pendulum configuration and BLDC motors operating as generators. The primary objective of the study was to develop a control strategy that enables the maximization of harvested power while simultaneously improving the energy conversion efficiency during the charging of the battery supplying the target system. The developed model incorporates the mechanical equations of motion of the double pendulum, an electrical model of the BLDC motors, and two independently controlled buck–boost converters, each connected to one joint of the pendulum. In addition, a perturb-and-observe (P&O) maximum power point tracking (MPPT) algorithm was implemented, which utilizes a portion of the computational resources of the target system's microcontroller and allows for dynamic adjustment of the electrical loads seen by the generators. Simulation results obtained in the Simulink environment confirm that the application of independent power converters combined with local MPPT control leads to an increase in the total harvested power and ensures more stable battery charging under conditions of variable mechanical excitation. The obtained results demonstrate the effectiveness of the proposed approach and indicate its potential applicability in self-powered systems operating in environments characterized by irregular and stochastic vibrations.

Keywords: energy harvesting; dual pendulum; BLDC generators; MPPT; nonlinear dynamics; buck–boost converter

Check for updates

Academic Editors: Nicolae Herisanu and Vasile Marinca

Received: 14 January 2026
Revised: 11 February 2026
Accepted: 16 February 2026
Published: 23 February 2026

Copyright: © 2026 by the authors. Licensee MDPI, Basel, Switzerland. This article is an open access article distributed under the terms and conditions of the Creative Commons Attribution (CC BY) license.

1. Introduction

In response to the growing demand for autonomous power-supply systems and the need to improve the energy efficiency of devices operating with limited access to conventional energy sources [1,2], mechanical vibration energy harvesting has become an important research direction [3–7]. Among the available concepts, harvesters based on nonlinear resonant structures [8–10]—including double-pendulum configurations [11–15]—are particularly promising because their complex dynamics can yield a broader operational bandwidth than linear resonators, enabling energy extraction over a wider range of excitation frequencies.

The practical relevance of such harvesters is closely linked to their integration with low-power electronics operating in an energy-autonomous mode, which underpins advanced monitoring systems, Internet of Things (IoT) nodes, and industrial infrastructure applications [7,16–18]. However, maximizing the net harvested energy in nonlinear, multi-degree-of-freedom harvesters remains challenging because the optimal electrical loading conditions vary with operating regime, excitation characteristics, and the instantaneous state of the mechanical system.

This study addresses this gap by presenting the modeling and control of a nonlinear vibration energy harvester based on a double pendulum in which mechanical energy is converted using brushless DC (BLDC) motors operating as generators. The harvester cooperates with a target device equipped with a microcontroller, and a portion of its computational resources is shared with the harvester to implement a maximum power point tracking (MPPT) algorithm [19–21]. The originality of the proposed approach lies in integrating MPPT directly into the harvester–device control architecture, enabling real-time adaptation of the generators' effective electrical load to the current electromechanical operating conditions [22]. As a result, the proposed strategy increases the harvested power and improves the efficiency of electrical energy conversion during battery charging [23].

An additional advantage of the considered double-pendulum harvester is that it can be excited not only by ambient vibrations of the host structure (e.g., industrial machinery, bridges, or vehicle components), but also by intentionally generated excitations [24–26], such as modulated electromagnetic actuation or impulsive kinematic impacts. This capability can extend the effective operating range of the system, particularly under low-amplitude or irregular vibration conditions.

A compact comparison with representative related works is provided in Table 1 to position the proposed double-pendulum harvester with integrated MPPT-based power management against prior pendulum-based and MPPT-enabled energy harvesting studies.

Table 1. Simplified comparison with related works.

Work	Focus/System	Pendulum/Nonlin.	MPPT/Power Mgmt
Elahi et al. [4]	Review: piezoelectric EH mechanisms	–	–
Muscat et al. [5]	Review: electromagnetic EH	–	(var.)
Wang [13]	Review: pendulum-based EH	yes	(var.)
Kumar et al. [12]	Double pendulum EH under base excitation	yes	–
Izadgoshasb et al. [14]	Double pendulum for human-motion EH (piezo)	yes	–
Chen et al. [25]	Chaotic pendulum hybrid harvester + sensing demo	yes	–
Gao et al. [26]	Dual-mass pendulum EM harvester	yes	–
Hoffmann et al. [16]	Self-adaptive EH system (adaptive interface)	–	yes
Lohrabi Pour et al. [21]	MPPT + cold start for ultra-low power EH	–	yes
This work	Double pendulum + BLDC generators + MPPT Algorithm	**yes**	**yes (integrated)**

Accordingly, this work develops a unified mathematical model combining the nonlinear double-pendulum dynamics, the BLDC generator model, and the power interface cooperating with the battery and control unit. Furthermore, a control algorithm enabling efficient MPPT and maintaining favorable generator operating conditions is proposed. Simulation and experimental results confirm that the proposed control strategy leads to a noticeable increase in the total harvested energy and improves conversion efficiency during charging processes.

2. Modeling and Control of a Nonlinear Double-Pendulum Energy Harvester

This section provides a detailed discussion of the modeling stages of a nonlinear energy harvesting system based on a double pendulum and integrated BLDC motors operating as generators [5,27,28]. The considered system performs the conversion of mechanical vibration energy into electrical energy, followed by its regulation using independently controlled buck–boost converters and an MPPT algorithm [19,20] implemented in a microcontroller. Due to the strong nonlinearities in the dynamics of the double pendulum and the nonlinear nature of the electromechanical coupling, each BLDC motor mounted at the pendulum joints is connected to a separate, independently controlled buck–boost converter. This configuration enables individual adjustment of the operating parameters of each generator–converter branch [29] to local mechanical conditions (oscillation amplitudes, angular velocities, and direction of motion), thereby maximizing the harvested power from both degrees of freedom of the system. Similar broadband benefits of multi-degree-of-freedom nonlinear architectures have also been reported for 2-DoF harvesters in different transduction mechanisms and nonlinear configurations [30,31].

2.1. System Description and Modeling Assumptions

The considered system consists of two pendulum links connected in series, each equipped with a BLDC motor integrated into the joint axis. The pendulum is mounted on a moving or vibrating base (e.g., a machine structure, vehicle frame, or shaker platform), which provides continuous vibrational excitation. The excitation vibrations are transmitted to the first pendulum link and subsequently to the second link, generating complex nonlinear motion [11,32] described by coupled differential equations of motion, which are presented in detail in Section 2.2. Such two-degree-of-freedom nonlinear systems can exhibit broadband responses due to modal interactions and, in tuned configurations, internal resonance phenomena [33,34]. The operation of the BLDC motors in generator mode enables electrical energy harvesting proportional to the angular velocities of the joints and the generated torque opposing the motion.

2.2. Formulation of the Mechanical Model for the Double Pendulum

The mechanical model of the system is presented in Figure 1. The system is composed of two oval-shaped pendulums joined at point B. The assembly is mounted on support at point A, which is capable of inducing excitation in the horizontal direction and, when required, in the vertical direction as well. The dimensions L_1 and L_2 define the length of the upper and lower parts of the pendulum, but s_1 and s_2 correspond to the center points of them, respectively. The system has two degrees of freedom and the coordinates ϕ_1 and

ϕ_2 are defined in vector form by Equation (1), where **i** and **j** represent the horizontal and vertical unit vectors.

$$\begin{aligned}\mathbf{q}_1 &= \Big(q_e + s_1 \sin\phi_1\Big)\mathbf{i} - \Big(q_e + s_1 \cos\phi_1\Big)\mathbf{j},\\ \mathbf{q}_2 &= \Big(q_e + L_1 \sin\phi_1 + s_2 \sin\phi_2\Big)\mathbf{i} - \Big(L_1 \cos\phi_1 + s_2 \cos\phi_2\Big)\mathbf{j},\end{aligned} \tag{1}$$

where the external excitation force is realized kinematically in horizontal directions only by harmonic functions $\mathbf{i}q_e = A_x \cos(\omega_e t)$. In general it is possible apply excitation in both directions through path curve as presented in Figure 2 activating functions $\mathbf{i}q_e$ and $\mathbf{j}q_e$, simultaneously.

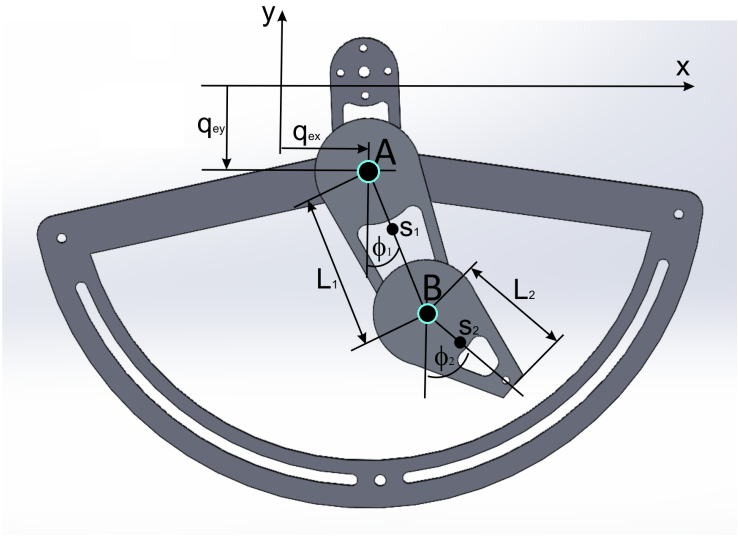
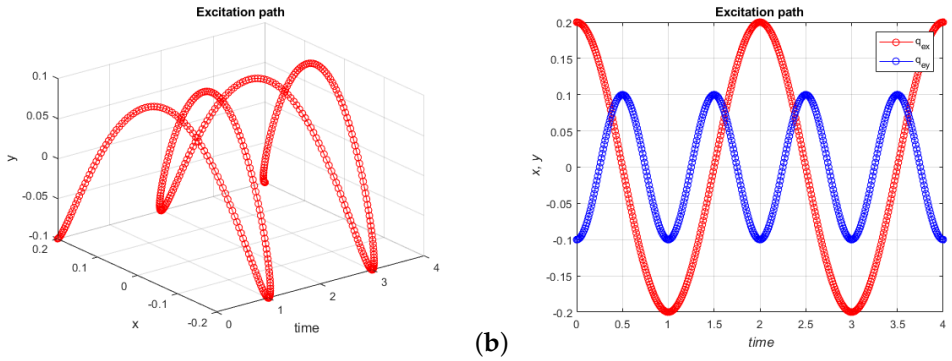


Figure 1. The schematic of the double pendulum system horizontally excited.



(**a**) (**b**)

Figure 2. The excitation paths in 3D (**a**) and 2D (**b**).

Applying the second kind Lagrange equations Equation (2) approach, the governing differential equations of motion are provided.

$$\frac{d}{dt}\left(\frac{\partial \mathbb{L}}{\partial \dot{q}_i}\right) - \frac{\partial \mathbb{L}}{\partial q_i} + \frac{\partial R}{\partial \dot{q}_i} = 0. \tag{2}$$

where $\mathbb{L} = T - \Pi$ is the Lagrangian, R is the Rayleigh dissipation function, and $\dot{q}_i$, q_i are generalized variables of velocities and displacements, from the formula of the position vector to the center of both pendulous of the system.

The kinetic T and potential Π energies of both pendulum parts are:

$$\begin{aligned} T_1 &= \frac{1}{2} m_1 \dot{\mathbf{q}}_1 \dot{\mathbf{q}}_1^T + \frac{1}{2} J_{s1} \dot{\phi_1}^2 = \frac{1}{2} m_1 \left(\dot{q}_{1x}^2 + \dot{q}_{1y}^2 \right) + \frac{1}{2} J_{s1} \dot{\phi_1}^2, \\ T_2 &= \frac{1}{2} m_2 \dot{\mathbf{q}}_2 \dot{\mathbf{q}}_2^T + \frac{1}{2} J_{s2} \dot{\phi_2}^2 = \frac{1}{2} m_2 \left(\dot{q}_{2x}^2 + \dot{q}_{2y}^2 \right) + \frac{1}{2} J_{s2} \dot{\phi_2}^2, \\ \Pi_1 &= m_1 g \mathbf{q}_{1y} = -m_1 g s_1 \cos \phi_1, \\ \Pi_2 &= m_2 g \mathbf{q}_{2y} = -m_2 g \left(L_1 \cos \phi_1 + s_2 \cos \phi_2 \right), \end{aligned} \tag{3}$$

where the m_1, m_2 correspond to the masses of both pendula and J_{s1}, J_{s2} represent the mass moment of inertia according the center points of its both parts.

Deriving the equations of motion using the Lagrange Equation (2) it is convenient to introduce the so-called Rayleigh dissipation function R defined as:

$$\begin{aligned} R_1 &= \frac{1}{2} \alpha_1 \dot{\phi}_1^2, \\ R_2 &= \frac{1}{2} \alpha_2 (\dot{\phi}_2 - \dot{\phi}_1)^2. \end{aligned} \tag{4}$$

The Rayleigh dissipation function is a common means of simplifying the derivation of the equation of motions in damped systems. In a sense, damping is treated just like kinetic and potential energy analytically. Introducing Equations (3) and (4) to Lagrangian Equation (2) and according to the derivations, the equations of motion are obtained as in Equation (5) in matrix form:

$$\begin{bmatrix} J_{11} & J_{12} \\ J_{21} & J_{22} \end{bmatrix} \begin{Bmatrix} \ddot{\phi}_1 \\ \ddot{\phi}_2 \end{Bmatrix} = \begin{Bmatrix} -\alpha_1 \dot{\phi}_1 - \alpha_2 (\dot{\phi}_1 - \dot{\phi}_2) - \dot{\phi}_2^2 m_2 L_1 s_2 \sin(\phi_1 - \phi_2) \\ -(m_1 s_1 + m_2 L_1) g \sin(\phi_1) + (m_1 s_1 + m_2 L_1) \ddot{q}_e \cos(\phi_1) \\ \\ \alpha_2 (\dot{\phi}_1 - \dot{\phi}_2) + \dot{\phi}_1^2 m_2 L_1 s_2 \sin(\phi_1 - \phi_2) \\ -m_2 s_2 g \sin(\phi_2) + m_2 s_2 \ddot{q}_e \cos(\phi_2) \end{Bmatrix} \tag{5}$$

where the corresponding inertia matrix $[J]$ reads

$$\begin{bmatrix} J_{11} & J_{12} \\ J_{21} & J_{22} \end{bmatrix} = \begin{bmatrix} J_{1A} + m_2 L_1^2 & m_2 L_1 s_2 \cos(\phi_1 - \phi_2) \\ m_2 L_1 s_2 \cos(\phi_1 - \phi_2) & J_{2B} \end{bmatrix} \tag{6}$$

The mass moments of inertia $J_{1A} = (J_{s1} + m_1 s_1^2)$ and $J_{2B} = (J_{s2} + m_2 s_2^2)$ for both parts of the pendulous with respect to the rotation points A and B which are calculated numerically by the FEM model (see Table 2).

Table 2. The system parameters.

Parameters	Values	Units
Length of the massless upper pendulum	$L_1 = 0.08$	m
Length of the massless lower pendulum	$L_2 = 0.05$	m
Mass of the upper tip mass	$m_1 = 0.099$	kg
Mass of the lower tip mass	$m_2 = 0.071$	kg
Center of the upper part	$s_1 = 0.044$	m
Center of the lower part	$s_2 = 0.0222$	m
Mass moment of inertia of the upper part	$J_{1A} = 0.000170$	kgm^2

Table 2. *Cont.*

Parameters	Values	Units
Mass moment of inertia of the lower part	$J_{2B} = 0.000064$	kgm^2
Damping coefficient of the upper part	$\alpha_1 = 0$	Nms/rad
Damping coefficient of the lower part	$\alpha_2 = 0.001$	Nms/rad
Horizontal excitation amplitude	$A_x = 0.2$	m
Vertical excitation amplitude	$A_y = 0$	m
The gravity acceleration	g = 9.81	m/s^2

By means of Lagrange approach, the differential equations of motion are derived and provided in matrix form:

$$\begin{bmatrix} J_{11} & J_{12} \\ J_{21} & J_{22} \end{bmatrix} \begin{Bmatrix} \ddot{\phi}_1 \\ \ddot{\phi}_2 \end{Bmatrix} = \begin{Bmatrix} C_1(t) \\ C_2(t) \end{Bmatrix} \tag{7}$$

where $[J]$ is the inertia matrix and matrix $\{C(t)\}$ reads:

$$\begin{Bmatrix} C_1(t) \\ \\ C_2(t) \end{Bmatrix} = \begin{Bmatrix} -\alpha_1\dot{\phi}_1 - \alpha_2(\dot{\phi}_1 - \dot{\phi}_2) - \dot{\phi}_2^2 m_2 L_1 s_2 \sin(\phi_1 - \phi_2) \\ -(m_1 s_1 + m_2 L_1) g \sin(\phi_1) + (m_1 s_1 + m_2 L_1)\ddot{q}_e \cos(\phi_1) \\ \\ \alpha_2(\dot{\phi}_1 - \dot{\phi}_2) + \dot{\phi}_1^2 m_2 L_1 s_2 \sin(\phi_1 - \phi_2) \\ -m_2 s_2 g \sin(\phi_2) + m_2 s_2 \ddot{q}_e \cos(\phi_2) \end{Bmatrix} \tag{8}$$

Transformations of equations for acceleration formula $\ddot{\phi}_1$ and $\ddot{\phi}_2$, it is necessary to determine the inverse inertia matrix $[J]^{-1}$. It required calculating the determinant of the inertia matrix $\det(J)$ and the transposed matrix of complements $([J]^D)^T$. The transposed inertia matrix of complements is:

$$([J]^D)^T = \left(\begin{bmatrix} J_{11} & J_{12} \\ J_{21} & J_{22} \end{bmatrix}^D \right)^T = \left(\begin{bmatrix} J_{22} & -J_{21} \\ -J_{12} & J_{11} \end{bmatrix} \right)^T = \begin{bmatrix} J_{22} & -J_{12} \\ -J_{21} & J_{11} \end{bmatrix} \tag{9}$$

These matrix operations lead to:

$$\begin{Bmatrix} \ddot{\phi}_1 \\ \ddot{\phi}_2 \end{Bmatrix} = \begin{bmatrix} J_{11} & J_{12} \\ J_{21} & J_{22} \end{bmatrix}^{-1} \begin{Bmatrix} C_1(t) \\ C_2(t) \end{Bmatrix} = \frac{1}{\det(J)} \begin{bmatrix} J_{22} & -J_{12} \\ -J_{21} & J_{11} \end{bmatrix} \begin{Bmatrix} C_1(t) \\ C_2(t) \end{Bmatrix} \tag{10}$$

Finally Equation (10) give the differential equation of motion for both pendulous, the angular acceleration of both the upper ϕ_1 and lower ϕ_2 parts of pendulum:

$$\begin{aligned} \ddot{\phi}_1 &= \frac{J_{22}C_1 - J_{12}C_2}{\det(J)} \\ \ddot{\phi}_2 &= \frac{J_{11}C_2 - J_{21}C_1}{\det(J)} \end{aligned} \tag{11}$$

The coupling with the BLDC motors is introduced through electromagnetic torques that depend on the angular velocities and the electrical load conditions.

The mechanical model was implemented in the Simulink environment as a subsystem block, in which the inputs are the electromagnetic torques and external excitations, while the outputs are the angular positions, angular velocities, and angular accelerations of the pendulum links.

2.3. Assumptions and Electromechanical Model of the BLDC Motor

This subsection presents the assumptions and the mathematical description of the electromechanical model of a three-phase BLDC motor operating as an electrical energy generator. The model is formulated in an averaged form and is intended for the analysis of system dynamics and the interaction of the motor with a diode rectifier and a DC-side load.

It is assumed that the considered BLDC motor is a symmetrical three-phase system with a trapezoidal back electromotive force (EMF) waveform, which is typical for this type of machine. On the electrical side, a three-phase diode rectifier is employed and modeled using an averaged representation. Magnetic saturation effects are neglected, and the electrical parameters of the windings, such as resistance, inductance, and the EMF constant, are assumed to be constant. Mechanical losses are described using a linear viscous friction model.

The mechanical part of the system is described by the rotor motion equation, in which the input variable is the driving torque T_m:

$$J\frac{d\omega}{dt} = T_m - T_e - B\omega, \tag{12}$$

where J denotes the moment of inertia, ω is the angular velocity of the rotor, B is the viscous friction coefficient, and T_e is the electromagnetic torque of the motor.

The electromagnetic torque is expressed as a function of the DC-side current of the rectifier:

$$T_e = k_t\, i_{dc}, \tag{13}$$

where k_t is the torque constant and i_{dc} is the DC-side current.

The averaged back electromotive force on the DC side is given by

$$e_{dc} = k_e\, \omega, \tag{14}$$

where k_e is the EMF constant of the motor.

The electrical subsystem on the DC side is described by the following equation:

$$L_{eq}\frac{di_{dc}}{dt} = e_{dc} - R_{eq}i_{dc} - v_{load}, \tag{15}$$

where L_{eq} and R_{eq} denote the equivalent inductance and resistance, respectively, and v_{load} is the load voltage. For a resistive load R_L, the following relationship holds:

$$v_{load} = R_L\, i_{dc}. \tag{16}$$

The state variables are defined as

$$x_1 = \omega, \qquad x_2 = i_{dc}. \tag{17}$$

Finally, the state-space representation of the model is given by

$$\begin{cases} \dot{\omega} = \frac{1}{J}(T_m - k_t i_{dc} - B\omega), \\ \dot{i}_{dc} = \frac{1}{L_{eq}}\left(k_e\omega - (R_{eq} + R_L)i_{dc}\right). \end{cases} \tag{18}$$

Representative output variables of the model include the angular velocity ω, the DC-side voltage

$$v_{dc} = R_L\, i_{dc}, \tag{19}$$

and the electrical power delivered to the load:

$$P = v_{dc}\, i_{dc}. \tag{20}$$

2.4. Robustness to Parameter Uncertainties

To assess the robustness of the proposed control strategy with respect to parameter uncertainties, a local (one-at-a-time) sensitivity analysis was performed by independently varying the main mechanical and electromechanical parameters around their nominal values: pendulum lengths (L_1, L_2), tip masses (m_1, m_2), damping coefficients (α_1, α_2), and generator constants (k_e, k_t). Each parameter was perturbed within $\pm 10\%$ of its nominal value (and $\pm 20\%$ as a stress case), while keeping the same excitation profile and MPPT settings. For each run, we computed: (i) the net harvested energy delivered to the DC bus/storage over the evaluation interval,

$$E_{\text{harv}} = \int_{t_0}^{t_1} v_{\text{dc}}(t)\, i_{\text{dc}}(t)\, dt, \tag{21}$$

and (ii) an MPPT effectiveness metric defined as the energy ratio relative to the nominal MPPT case,

$$\eta_{\text{MPPT}} = \frac{E_{\text{harv}}}{E_{\text{harv,nom}}}. \tag{22}$$

The results indicate that the harvested energy is most sensitive to the damping coefficients and the generator constants, which directly affect mechanical dissipation and electromechanical coupling. In contrast, variations in lengths and masses primarily shift the dynamical response and the operating regimes encountered under base excitation, leading to moderate changes in harvested energy. Importantly, across the tested uncertainty ranges the MPPT loop remained stable (i.e., without oscillatory behavior or loss of tracking), and the relative performance gain of MPPT over a fixed-load strategy was preserved. Overall, these observations suggest that the proposed control strategy is robust to realistic parameter variations stemming from manufacturing tolerances, mounting conditions, and aging.

2.5. DC–DC Converter Model and Parameters

Each BLDC generator is interfaced with an independently controlled buck–boost DC–DC converter to enable dynamic load adaptation via the MPPT algorithm. The converter model used in simulations includes the main non-idealities relevant to low-power operation, i.e., conduction losses of the switching device and the diode. A schematic of the implemented converter stage is shown in Figure 3.

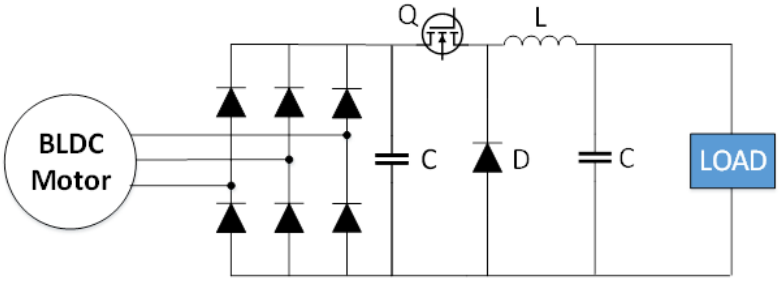


Figure 3. Schematic of the buck–boost DC–DC converter used as the power interface for each generator branch.

2.6. Control Architecture and MPPT Implementation

Figure 4 presents the overall control architecture of the proposed energy harvesting system. Each BLDC generator branch is interfaced through an independent rectifier and a buck–boost DC–DC converter. The microcontroller measures the electrical variables on the DC side and executes the MPPT routine, which updates the converter duty cycle to adapt the effective electrical load seen by the generator. This decoupled, two-branch structure enables independent optimization of the energy extraction from both degrees of freedom. From a broader perspective, broadband energy harvesting in multi-DoF nonlinear systems can be achieved either without internal resonance [30] or by deliberate tuning to internal resonance conditions [33,34]; the proposed MPPT-based interface is compatible with both approaches.

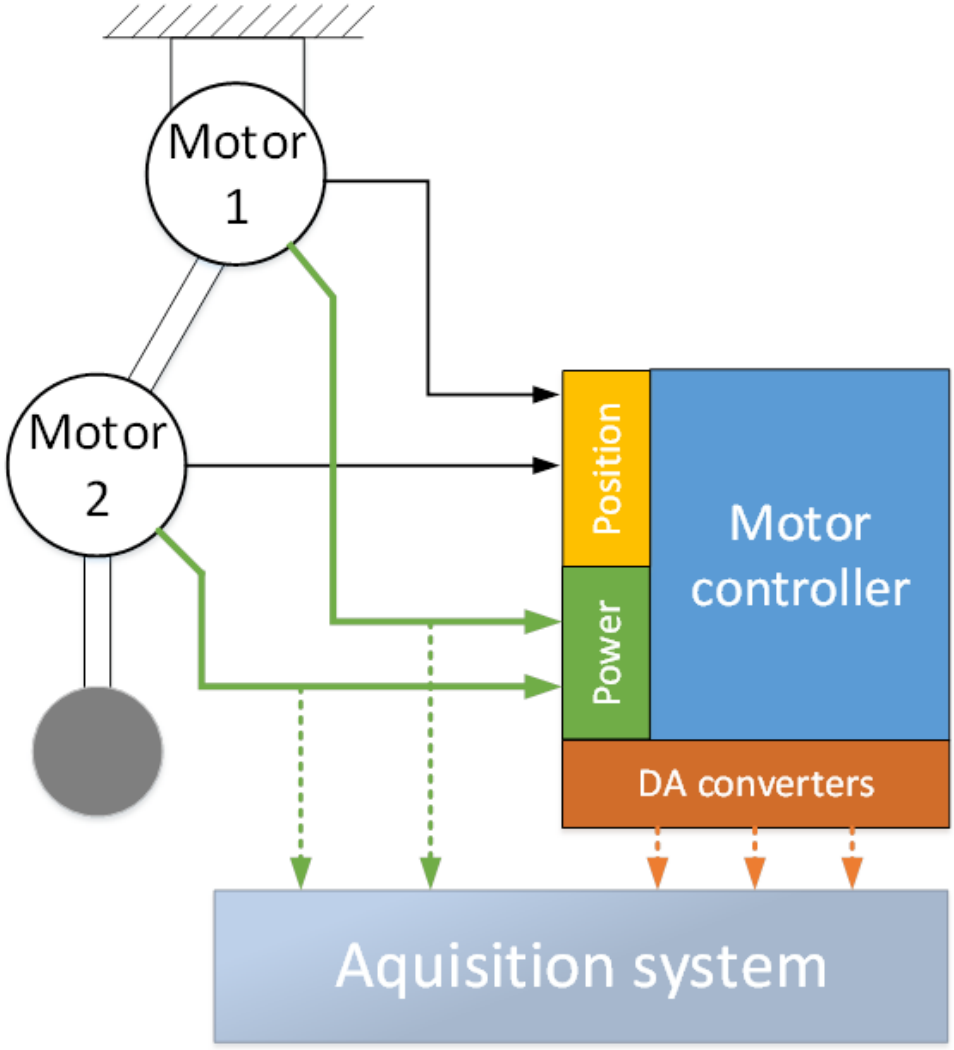


Figure 4. Control scheme of the energy harvester: sensing, MPPT computation, and independent duty-cycle control for each generator–converter branch.

2.7. Remarks on Analytical Solutions and Internal Resonance

The double-pendulum harvester exhibits strongly nonlinear dynamics and may operate in regime-switching responses (including broadband and potentially chaotic motions), especially under base excitation and electromechanical coupling. Therefore, while approximate analytical techniques such as harmonic balance or multi-scale methods can be valuable for weakly nonlinear, near-periodic oscillations, they become less informative for the operating conditions targeted in this work (broadband response, multiple harmon-

ics, and closed-loop power-electronic control). For this reason, the proposed method is evaluated primarily using time-domain simulations, which directly capture the interaction between nonlinear mechanics, rectification, DC–DC conversion, and MPPT control.

Since the device is a two-degree-of-freedom system, modal interactions and internal resonance conditions (e.g., 1:1 or 2:1) can potentially broaden the harvesting bandwidth in appropriately tuned configurations. Such mechanisms have been successfully used to enhance broadband harvesting in related nonlinear systems [33,34]. Although internal resonance tuning is not the focus of the present study, the proposed modeling and control framework is compatible with such extensions by modifying the mechanical design parameters to target desired modal frequency ratios and then applying the same MPPT-based load adaptation strategy. In addition, broadband responses can also be obtained without internal resonance in properly designed 2-DoF nonlinear architectures [30], and in other broadband harvesting contexts such as flow-induced systems [35]. These avenues can be considered for future optimization of the harvester design.

3. Results

In this section, the simulation results of the dual-pendulum energy harvesting system are presented for two amplitudes of kinematic excitation, $A_x = 0.04$ and $A_x = 0.08$, within the frequency range of 8–13 Hz. These values correspond to the horizontal excitation amplitude defined in Table 2 (with $A_y = 0$ in the considered cases). For each excitation amplitude, two variants of the power electronic interface are compared: a buck–boost converter controlled by an MPPT algorithm and a reference configuration with a fixed duty cycle (Duty = 0.9). The analysis focuses on the electrical energy harvested from the two generators corresponding to the first and second pendulum links.

For the lower excitation amplitude ($A_x = 0.04$), the electrical energy harvested from the first motor remains at a comparable level across the entire analyzed frequency range, regardless of the applied control strategy. Both in the MPPT-controlled case and in the reference configuration, only minor variations in the harvested energy are observed with increasing excitation frequency. This indicates that, at low excitation amplitudes, the first motor operates under relatively stable electromechanical coupling conditions, and its contribution to the overall energy balance of the system is limited. In contrast, for the second motor at $A_x = 0.04$, a more pronounced influence of the MPPT algorithm is observed. Across the entire frequency band, the energy harvested in the MPPT-controlled case exceeds that obtained in the reference configuration, with the relative energy gain typically ranging from several tens of percent. This demonstrates that even at small excitation amplitudes, dynamic matching of the electrical load enables more efficient utilization of the mechanical energy available in the second degree of freedom of the dual-pendulum system.

A markedly different behavior is observed for the higher excitation amplitude ($A_x = 0.08$). In this case, a substantial increase in the harvested electrical energy is evident, particularly when MPPT control is applied. For both motors, the energy response exhibits increased sensitivity to the excitation frequency, indicating stronger nonlinear effects in the system dynamics. At the same time, the application of the MPPT algorithm leads to a significant enhancement of the harvested energy compared to the reference case, with especially pronounced differences at selected excitation frequencies. For $A_x = 0.08$ under MPPT control, distinct maxima of harvested electrical energy appear at frequencies around 9 Hz and 13 Hz, along with an additional maximum near 11 Hz. These peaks are not present in the configuration with a fixed duty cycle, suggesting the emergence of additional resonance regions activated by dynamic electrical load control. At these frequencies, a rapid increase in the energy harvested from the second motor is observed, which accounts for the dominant contribution to the total electrical energy gain of the

system. The first motor also exhibits increased energy output in the resonance regions; however, its contribution remains smaller compared to that of the second generator.

The analysis of the relative energy gain resulting from the application of MPPT further confirms these observations. For both excitation amplitudes, the MPPT algorithm provides a positive energy gain across the entire analyzed frequency range. For $A_x = 0.04$, this gain is moderate and primarily results from improved performance of the second motor. For $A_x = 0.08$, the relative energy gain increases significantly in the vicinity of resonance frequencies, in particular at 9 Hz, 11 Hz, and 13 Hz, reaching values several times higher than those observed outside these regions. These results clearly demonstrate the crucial role of the MPPT algorithm in activating favorable dynamic states of the system.

In summary, the simulation results indicate that the excitation amplitude has a significant influence on the energy harvesting characteristics of the dual-pendulum system. For low excitation amplitudes, the improvement in energy harvesting efficiency achieved through MPPT is moderate and mainly associated with the second motor. For higher excitation amplitudes, the MPPT algorithm not only increases the amount of harvested energy, but also induces additional resonance regions, including one around 11 Hz, which substantially enhance the total electrical energy output of the system.

4. Discussion

The conducted simulations clearly demonstrate that the application of a buck–boost converter controlled by an MPPT algorithm in a dual-pendulum-based energy harvesting system has a significant impact not only on the level of harvested electrical energy, but also on the dynamic characteristics of the entire electromechanical system. The obtained results confirm that the system should be regarded as a strongly coupled mechanical–electrical system, in which modifications in the power electronic subsystem may induce qualitatively new dynamic states on the mechanical side [36–38]. In particular, the comparison of absolute harvested energy for the MPPT-controlled interface and the fixed-duty reference in Figure 5 shows an increase in total harvested electrical energy by approximately 20–30% over a wide range of excitation frequencies. This improvement results primarily from the ability to dynamically match the electrical load of the generators to the instantaneous operating conditions. In contrast to the configuration with a fixed duty cycle, the MPPT algorithm enables continuous adjustment of the operating point to varying generator voltages and currents, thereby reducing the time intervals during which the system operates away from the maximum power point. This effect becomes particularly important in nonlinear systems, where the dynamic response exhibits substantial variability even under constant excitation parameters.

One of the most important conclusions drawn from the analysis is the emergence of additional resonance regions at excitation frequencies of approximately 9 Hz and 13 Hz in the MPPT-controlled configuration. These resonances are not observed in the reference case and are not associated with changes in the mechanical parameters of the system, but rather with modifications of the electromechanical coupling conditions. The dynamically adjusted electrical load affects the effective damping of the generators, which in turn alters the system energy balance and enables the excitation of dynamic states that remain inaccessible under passive loading conditions. The corresponding effect is also reflected in the relative MPPT gain shown in Figure 6, where the gain increases notably in the vicinity of these resonance frequencies.

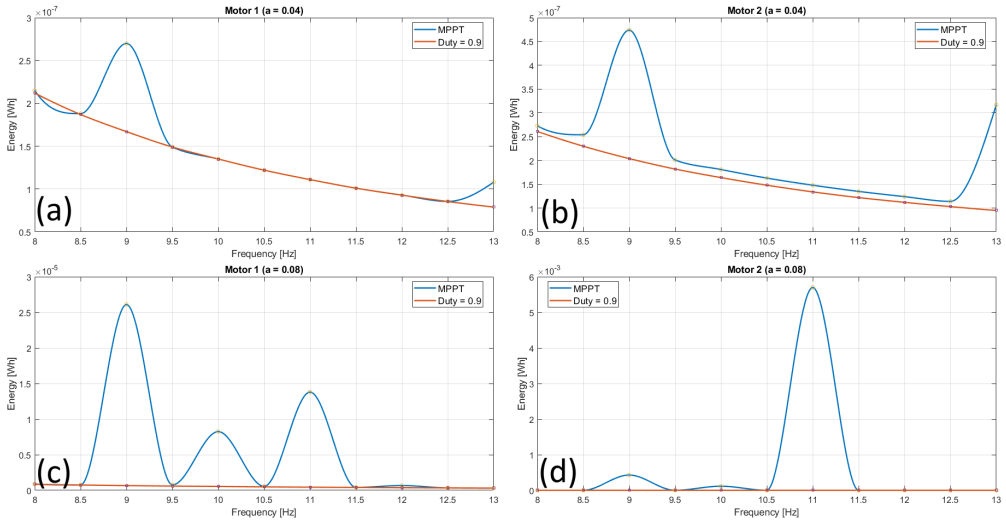


Figure 5. Absolute harvested electrical energy (delivered to the DC bus/storage) versus excitation frequency for MPPT control and the fixed duty-cycle reference (Duty = 0.9). (**a**) Motor 1, $A_x = 0.04$, (**b**) Motor 2, $A_x = 0.04$, (**c**) Motor 1, $A_x = 0.08$, (**d**) Motor 2, $A_x = 0.08$.

An analysis of the energy distribution between the two generators reveals a pronounced asymmetry in their roles within the energy harvesting process. Outside the resonance regions, the electrical energy harvested from the first motor remains nearly constant (Figure 5a,c), indicating its relatively stable interaction with the mechanical subsystem. In contrast, the increase in total harvested energy observed in the MPPT configuration outside resonance regions is mainly attributable to the enhanced energy harvested from the second motor (Figure 5b,d). This behavior can be associated with the location of the second generator within the dual-pendulum structure and its greater sensitivity to nonlinear dynamic effects, such as variations in amplitude and angular velocity of the second pendulum link.

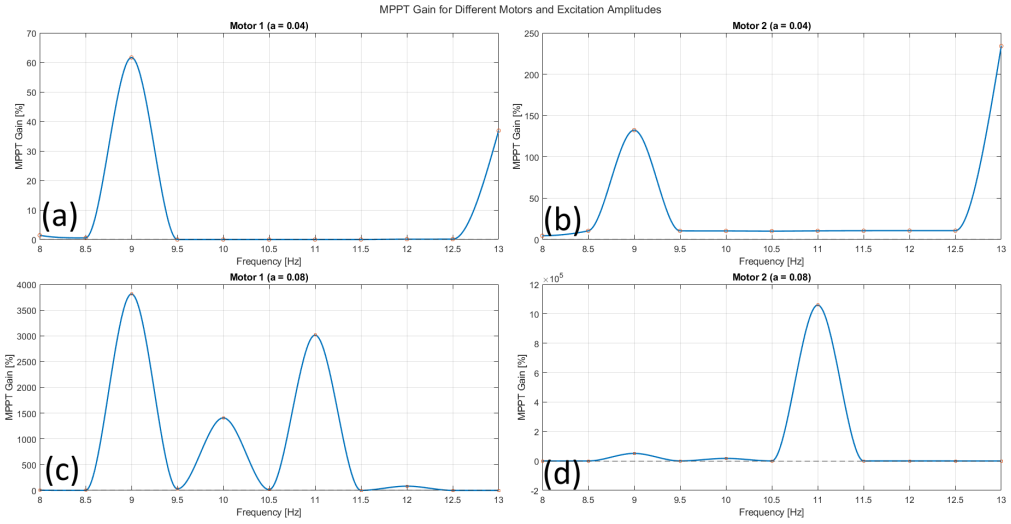


Figure 6. Relative gain in harvested electrical energy obtained with MPPT control compared to the fixed duty-cycle reference (Duty = 0.9), expressed as a percentage. (**a**) Motor 1, $A_x = 0.04$, (**b**) Motor 2, $A_x = 0.04$, (**c**) Motor 1, $A_x = 0.08$, (**d**) Motor 2, $A_x = 0.08$.

Within the resonance regions, the differences between the two configurations are further amplified. The application of MPPT leads to a simultaneous increase in the energy harvested from both motors at these frequencies; however, the dominant contribution still originates from the second generator. This observation suggests that effective exploitation

of resonances in multi-generator systems may require an uneven distribution of energy harvesting functions among individual sources.

From the perspective of practical applications, the obtained results indicate that active power electronic control can significantly broaden the effective operating bandwidth of energy harvesting systems without the need to modify their mechanical structure. The ability to activate additional resonance regions through MPPT control allows for more efficient utilization of variable and difficult-to-predict excitations, which is particularly relevant in applications involving environmental vibrations or irregular motion.

It should be noted that the presented results are based on a numerical model and assumptions regarding the operation of the power converter and the MPPT algorithm. Future studies should address switching losses, dynamic limitations of the control system, and experimental validation. Nevertheless, the obtained results confirm that the integration of MPPT algorithms with nonlinear mechanical systems represents a promising direction for the development of energy harvesting systems with enhanced efficiency and an extended operational bandwidth.

5. Conclusions

This work investigated a nonlinear dual-pendulum vibration energy harvester equipped with two BLDC motors operating as generators and an actively controlled power-electronic interface. A unified modeling framework was developed to capture the coupled dynamics of the mechanical subsystem, the electromechanical generator behavior, and the DC-side power interface with maximum power point tracking (MPPT). The main contributions can be summarized as follows:

1. A coupled electromechanical model of a two-degree-of-freedom nonlinear double-pendulum harvester was formulated and implemented in a simulation environment, including an averaged BLDC generator model and its interaction with the DC-side load.
2. A dual-branch power interface was introduced, where each generator is connected to an independently controlled buck–boost converter, enabling branch-level adaptation to local operating conditions of the two joints.
3. An MPPT-based control strategy was integrated into the energy harvesting architecture and described as a discrete-time duty-cycle update procedure with saturation constraints. The converter model used in the simulations includes key non-idealities relevant to low-power operation (conduction losses of switching and diode elements).
4. A brief robustness assessment was conducted via a local (one-at-a-time) sensitivity study of the main mechanical and electromechanical parameters. The results indicate that the MPPT loop remained stable under realistic parameter perturbations and that the relative advantage of MPPT over a fixed-duty reference was preserved.

The simulation study shows that MPPT control increases the harvested electrical energy across the analyzed frequency band for the considered excitation levels. For higher excitation amplitude, the MPPT-controlled interface also activates additional favorable operating regions (resonance-like peaks) that are not observed for the fixed-duty reference case, demonstrating that electrical load adaptation can influence the accessible dynamic states of the nonlinear harvester.

Several limitations of the present study should be noted. First, the results are primarily based on numerical simulations with averaged electromechanical and power-electronic models; although conduction losses are included, additional effects such as detailed switching losses, high-frequency ripple, thermal effects, and measurement noise were not explicitly modeled. Second, the mechanical model relies on nominal parameters obtained for the considered prototype geometry, and further experimental identification would be beneficial

for precise quantitative prediction. Third, the MPPT procedure was evaluated for the considered excitation range and harvester configuration; broader validation under different vibration spectra and additional mechanical tuning (e.g., intentional internal resonance design) remains a topic for future work. Finally, extended experimental validation with real hardware and long-term operation is required to fully assess efficiency, robustness, and practical applicability.

Future work will therefore focus on (i) experimental verification of the complete electromechanical system under realistic excitations, (ii) inclusion of detailed converter switching models and efficiency mapping, and (iii) systematic exploration of design variants (scaling, parameter tuning, and potential internal resonance conditions) combined with MPPT-based load adaptation for application-specific vibration spectra.

Author Contributions: Conceptualization, M.F., M.B. and G.L.; Methodology, M.F., M.B. and M.W.; Software, M.F.; Validation, M.B., G.L., K.K. and M.W.; Formal analysis, M.B. and G.L.; Investigation, M.F. and K.K.; Resources, K.K.; Data curation, M.F. and K.K.; Writing—original draft, M.F., M.B. and G.L.; Writing—review & editing, M.B., G.L. and K.K.; Visualization, M.F. and M.W.; Supervision, G.L.; Project administration, M.F. All authors have read and agreed to the published version of the manuscript.

Funding: This research was funded by the National Science Centre, Poland under the OPUS Call in the Weave program under project no. 2023/51/I/ST8/02739.

Data Availability Statement: The data that supports the findings of this study areis available from the corresponding author, upon reasonable request.

Conflicts of Interest: The authors declare no conflicts of interest

References

1. Jiang, Z.; Yang, Z. A Smart Energy Management Strategy of an Energy Harvesting System for Industrial Wireless Sensor Nodes. *Energies* **2022**, *15*, 8674. [CrossRef]
2. Park, S.; Lee, H. Intelligent Control of Energy Harvesting Systems for Enhanced Performance under Variable Excitation. *Energies* **2024**, *17*, 3469. [CrossRef]
3. Malaji, P.V.; Ali, S.F.; Litak, G. Energy Harvesting: Materials, Structures and Methods. *Eur. Phys. J. Spec. Top.* **2022**, *231*, 1355–1358. [CrossRef]
4. Elahi, H.; Eugeni, M.; Gaudenzi, P. A Review on Mechanisms for Piezoelectric-Based Energy Harvesters. *Energies* **2018**, *11*, 1850. [CrossRef]
5. Muscat, A.; Bhattacharya, S.; Zhu, Y. Electromagnetic Vibrational Energy Harvesters: A Review. *Sensors* **2022**, *22*, 5555. [CrossRef]
6. Sun, R.; Zhou, S.; Cheng, L. Ultra-Low Frequency Vibration Energy Harvesting: Mechanisms, Enhancement Techniques, and Scaling Laws. *Energy Convers. Manag.* **2023**, *276*, 116585. [CrossRef]
7. Gazkooh, H.K.; Sadhu, A.; Liu, K. Vibration-Based Energy Harvesting in Large-Scale Civil Infrastructure: A Comprehensive Outlook of Current Technologies and Future Prospects. *Discov. Civ. Eng.* **2025**, *2*, 154. [CrossRef]
8. Giri, A.M.; Ali, S.F.; Arockiarajan, A. Dynamics of Symmetric and Asymmetric Potential Well-Based Piezoelectric Harvesters: A Comprehensive Review. *J. Intell. Mater. Syst. Struct.* **2021**, *32*, 1881–1947. [CrossRef]
9. Liu, H.; Zhao, L.; Chang, Y.; Cong, C. Design and Characteristic Analysis of Magnetostrictive Bistable Vibration Harvester with Displacement Amplification Mechanism. *Energy Convers. Manag.* **2021**, *243*, 114361. [CrossRef]
10. Hua, C.; Zou, D.; Cao, G. Improving Low-Frequency Vibration Energy Harvesting of a Piezoelectric Cantilever with Quasi-Zero Stiffness Structure: Theory and Experiment. *Actuators* **2025**, *14*, 93. [CrossRef]
11. Shinbrot, T.; Grebogi, C.; Wisdom, J.; Yorke, J.A. Chaos in a Double Pendulum. *Am. J. Phys.* **1992**, *60*, 491–499. [CrossRef]
12. Kumar, R.; Gupta, S.; Ali, S.F. Energy Harvesting from Chaos in Base Excited Double Pendulum. *Mech. Syst. Signal Process.* **2019**, *124*, 49–64. [CrossRef]
13. Wang, T. Pendulum-Based Vibration Energy Harvesting: Mechanisms, Transducer Integration, and Applications. *Energy Convers. Manag.* **2023**, *276*, 116469. [CrossRef]
14. Izadgoshasb, I.; Lim, Y.Y.; Tang, L.; Padilla, R.V.; Tang, Z.S.; Sedighi, M. Improving Efficiency of Piezoelectric Based Energy Harvesting from Human Motions Using Double Pendulum System. *Energy Convers. Manag.* **2019**, *184*, 559–570. [CrossRef]

15. Kecik, K.; Mitura, A. Energy Recovery from a Pendulum Tuned Mass Damper with Two Independent Harvesting Sources. *Int. J. Mech. Sci.* **2020**, *174*, 105568. [CrossRef]
16. Hoffmann, D.; Willmann, A.; Hehn, T.; Folkmer, B.; Manoli, Y. A Self-Adaptive Energy Harvesting System. *Smart Mater. Struct.* **2016**, *25*, 035013. [CrossRef]
17. Lee, S.; Cho, K.K.N. Sustainability Assessment of Vibration Energy Harvesting Systems in Smart Cities. *Sustainability* **2023**, *15*, 10252. [CrossRef]
18. Zhang, X.; Huang, H. Assessment of Energy Harvesting Strategies for Sustainable Sensor Networks. *Sustainability* **2023**, *15*, 11144. [CrossRef]
19. Abdel-Rahim, O.; Wang, H. A New High Gain DC–DC Converter with Model-Predictive-Control Based MPPT Technique for Photovoltaic Systems. *CPSS Trans. Power Electron. Appl.* **2020**, *5*, 191–200. [CrossRef]
20. Miao, J.; Chen, H.; Lei, Y.; Lv, Y.; Liu, W.; Song, Z. MPPT Circuit Using Time Exponential Rate Perturbation and Observation for Enhanced Tracking Efficiency for a Wide Resistance Range of Thermoelectric Generator. *Appl. Sci.* **2021**, *11*, 4650. [CrossRef]
21. Lohrabi Pour, F.; Hong, S.K.; Lee, J.; Sohani Darban, M.; Kim, J.M.; Ha, D.S. Three-Phase Powerline Energy Harvesting Circuit with Maximum Power Point Tracking and Cold Start-Up. *Appl. Sci.* **2025**, *15*, 11954. [CrossRef]
22. Lee, J.; Chun, Y.; Kim, J.; Park, B. An Energy-Harvesting System Using MPPT at Shock Absorber for Electric Vehicles. *Energies* **2021**, *14*, 2552. [CrossRef]
23. Liu, C.; Wu, B. Microstructural Effects on Vibration Energy Harvesting Using MEMS Cantilevers. *Micromachines* **2021**, *11*, 1009. [CrossRef]
24. Luo, A.; Xu, W.; Sun, J.; Xi, K.; Tang, S.; Guo, X.; Lee, C.; Wang, F. Vibration Energy Harvester with Double Frequency-Up Conversion Mechanism for Self-Powered Sensing System in Smart City. *Nano Energy* **2023**, *105*, 108030. [CrossRef]
25. Chen, X.; Gao, L.; Chen, J.; Lu, S.; Zhou, H.; Wang, T.; Wang, A.; Zhang, Z.; Guo, S.; Mu, X.; et al. A Chaotic Pendulum Triboelectric–Electromagnetic Hybridized Nanogenerator for Wave Energy Scavenging and Self-Powered Wireless Sensing System. *Nano Energy* **2020**, *69*, 104440. [CrossRef]
26. Gao, C.; Su, X.; Tang, J.; Liu, D.; Liu, J. The Electromagnetic Vibration Energy Harvesters Utilize Dual-Mass Pendulums for Multidirectional Harvesting. *Sensors* **2025**, *25*, 2017. [CrossRef]
27. Malaji, P.V.; Ali, S.F. Magneto-Mechanically Coupled Electromagnetic Harvesters for Broadband Energy Harvesting. *Appl. Phys. Lett.* **2017**, *111*, 083901. [CrossRef]
28. Qadeer, A.; Azam, M.; Abdul, B.; Asary, A.R. Micro-Electromagnetic Vibration Energy Harvesters: Analysis and Comparative Assessment. *Mater. Proc.* **2025**, *25*, 10. [CrossRef]
29. Umar, D.A.; Alkawsi, G.; Jailani, N.L.M.; Alomari, M.A.; Baashar, Y.; Alkahtani, A.A.; Capretz, L.F.; Tiong, S.K. Evaluating the Efficacy of Intelligent Methods for Maximum Power Point Tracking in Wind Energy Harvesting Systems. *Processes* **2023**, *11*, 1420. [CrossRef]
30. Zhang, X.F.; Yang, L.; Jiang, W.A.; Jing, X.J.; Chen, L.Q. Broadband Energy Harvesting in a Two-Degree-of-Freedom Nonlinear System without Internal Resonance. *J. Intell. Mater. Syst. Struct.* **2024**, *35*, 17–28. [CrossRef]
31. Li, J.; Zhang, X.; Jiang, W.; Bi, Q.; Chen, L. A Novel Cut-Out Piezoelectric Beam with Limiters for Broadband Energy Harvesting. *Int. J. Non-Linear Mech.* **2024**, *167*, 104919. [CrossRef]
32. Awrejcewicz, J.; Kudra, G.; Wasilewski, G. Experimental and Numerical Investigation of Chaotic Regions in the Triple Physical Pendulum. *Nonlinear Dyn.* **2007**, *50*, 755–766. [CrossRef]
33. Jiang, W.A.; Ma, X.D.; Han, X.J.; Chen, L.Q.; Bi, Q.S. Broadband Energy Harvesting Based on One-to-One Internal Resonance. *Chin. Phys. B* **2020**, *29*, 100503. [CrossRef]
34. Jiang, W.; Han, X.; Chen, L.; Bi, Q. Improving Energy Harvesting by Internal Resonance in a Spring-Pendulum System. *Acta Mech. Sin.* **2020**, *36*, 618–623. [CrossRef]
35. Wu, T.Y.; Jiang, W.A.; Chen, L.Q.; Bi, Q.S. A Broadband Flow Energy Harvester Induced by the Wake of a Bluff Body. *Eur. Phys. J. Plus* **2022**, *137*, 650. [CrossRef]
36. Yurchenko, D.; Alevras, P.; Zhou, S.; Wang, J.; Litak, G.; Gaidai, O.; Ye, R. Nonlinear Vibration Mitigation of a Crane's Payload Using Pendulum Absorber. *Mech. Syst. Signal Process.* **2021**, *156*, 107558. [CrossRef]
37. Malaji, P.V.; Friswell, M.I.; Adhikari, S. High-Energy Orbit Harvesting with Torsionally Coupled Mistuned Pendulums. *J. Vib. Eng. Technol.* **2022**, *11*, 4223–4240. [CrossRef]
38. Margielewicz, J.; Gaska, D.; Litak, G.; Wolszczak, P.; Zhou, S. Energy Harvesting in a System with a Two-Stage Flexible Cantilever Beam. *Sensors* **2022**, *22*, 7399. [CrossRef]

Disclaimer/Publisher's Note: The statements, opinions and data contained in all publications are solely those of the individual author(s) and contributor(s) and not of MDPI and/or the editor(s). MDPI and/or the editor(s) disclaim responsibility for any injury to people or property resulting from any ideas, methods, instructions or products referred to in the content.